IVYSPRING INTERNATIONAL PUBLISHER

Theranostics

2018; 8(7): 1879-1891. doi: 10.7150/thno.22070

Research Paper

Ultrasound Molecular Imaging of Atherosclerosis for Early Diagnosis and Therapeutic Evaluation through Leucocyte-like Multiple Targeted Microbubbles

Fei Yan[1*], Yu Sun[2, 3*], Yang Mao[4], Meiying Wu[1], Zhiting Deng[1], Shuai Li[1], Xin Liu[1], Li Xue[2]✉, Hairong Zheng[2]✉

1. Paul C. Lauterbur Research Center for Biomedical Imaging, Institute of Biomedical and Health Engineering, Shenzhen Institutes of Advanced Technology, Chinese Academy of Sciences, Shenzhen 518055 China
2. Ultrasound Room, Department of Cardiology, Fourth Affiliated Hospital of Harbin Medical University, Harbin 150001, China
3. Department of Ultrasonography, Shenzhen People's Hospital, Second Clinical Medical College of Jinan University, Shenzhen, 518020, China.
4. The Key Laboratory of Cardiovascular Remodeling and Function Research, Chinese Ministry of Education and Chinese Ministry of Health, The State and Shandong Province Joint Key Laboratory of Translational Cardiovascular Medicine, Qilu Hospital of Shandong University, Jinan, Shandong, 250012, PR China.

*Both authors contributed equally to this manuscript.

✉ Corresponding authors: Li Xue and Hairong Zheng, E-mails: toxueli@163.com and hr.zheng@siat.ac.cn, Telephone: +86 755 86392284, Fax: +86 755 96382299.

Received: 2017.07.25; Accepted: 2018.01.02; Published: 2018.02.14

Abstract

Cardiovascular diseases resulting from atherosclerosis have become a serious threat to human health. It is well-known that an ongoing inflammatory response is involved during atherosclerosis progression that ultimately results in the accumulation of lipids and formation of plaques. Monitoring the pathological changes during the inflammatory response will be of great significance for early diagnosis and therapeutic evaluation of atherosclerosis. Targeted contrast-enhanced ultrasonography has been shown to be a promising noninvasive imaging technique for evaluating the degree of atherosclerosis and may potentially be translated to clinical imaging in the future. However, inadequate cell adhesion of targeted microbubbles (MBs) in large arterial vessels still remains a great challenge.

Methods: By mimicking the leucocytes that are recruited to the vessel wall during the initiation of atherosclerosis through selectin-dependent arrest and cell adhesion molecule-mediated firm cell adhesion, we developed VCAM-1/ICAM-1/P-selectin-targeted MB_{VIS} by integrating VCAM-1 and ICAM-1 antibodies and synthetic polymeric sialyl Lewis X (sLe^x) onto the MB surface.

Results: The resulting MB_{VIS} had a high affinity to inflammatory bEnd.3 cells in both static and dynamic flow conditions. Significantly enhanced ultrasound imaging signals were achieved by MB_{VIS} in detecting the atherosclerosis progress when compared with the single- or dual-targeted MBs. Taking advantage of the artificial MB_{VIS}, less ultrasound imaging signals were found in the atorvastatin-treated, but not placebo-treated, ApoE-deficient mice with atherosclerosis, revealing a potential therapeutic efficacy of atorvastatin for early stage atherosclerosis. This was further confirmed by histologic staining examination.

Conclusions: Our study provides a promising ultrasound molecular imaging probe for early-stage diagnosis and therapeutic evaluation of atherosclerosis.

Key words: Ultrasound molecular imaging; Therapeutic evaluation; Atherosclerosis; Targeted microbubbles

Introduction

Cardiovascular disease is a leading cause of death worldwide [1]. The underlying cause of the cardiovascular event is atherosclerosis-a chronic inflammatory disease, characterized by intimal plaques of the arterial vessels that may undergo spontaneous rupture with subsequent heart attack or

stroke [2, 3]. During the initiation and progression of atherosclerosis, inflammatory leucocytes recruit to the vessel wall and subsequently transmigrate into the underlying tissue in response to infection or injury [4]. In the multistep adhesion cascade, many specifically overexpressed factors such as selectins, integrins, and cell adhesion molecules (CAMs) participate and play key roles in the inflammatory reaction [5]. The upregulation of selectins, intercellular adhesion molecule 1 (ICAM-1) and vascular cell adhesion molecule 1 (VCAM-1) greatly increase leucocyte and inflammatory cell adhesion on the endothelium. In brief, selectins function as initiators of leucocyte adhesion and signaling at the vascular wall [6]. They interact with O-glycosylated carbohydrate ligands on P-selectin glycoprotein ligand-1 (PSGL-1) expressed on all monocytes. This interaction allows leucocytes to roll on the endothelium and negotiate the high shear stress. Also, selectin signals induce extension of the αLβ2 ectodomain from a closed headpiece [7]. This conformation change produces intermediate affinity for ICAM-1 and mediates slow rolling but not arrest. VCAM-1 can bind to very late antigen-4 (VLA-4) and mediates slow rolling on cytokine-activated endothelium, thus facilitating the transition between rolling and firm arrest [8]. Therefore, selectins, VCAM-1 and ICAM-1, which occur at the inflammatory injury site in the original multistep atherosclerosis paradigm, are widely regarded as good targets for molecular imaging of early-stage atherosclerosis and biomarkers for therapeutic evaluation in anti-atherosclerosis treatments [9].

To date, several imaging platforms have been used for molecular imaging, including magnetic resonance imaging (MRI), positron emission tomography (PET), single-photon emission computed tomography (SPECT), optical imaging and ultrasound. Some of these are already being used in clinical practice (diagnosis or therapeutic evaluation), whereas others are currently at advanced development stages. Among them, ultrasound molecular imaging using targeted microbubbles (MBs) has been shown to be a promising non-invasive molecular imaging technique, especially for cardiovascular diseases [10-12]. MBs are relatively large in size (about 1-5 μm diameter), which limits them to the vascular system and meanwhile gives them a higher chance to attach to their targets than smaller probes [13]. In addition, ultrasound is real-time, has high temporal resolution, and does not involve ionizing radiation. Moreover, ultrasound imaging is a low-cost modality, with scanners generally available in hospitals and many outpatient settings. Recently, ultrasound molecular imaging has been used to image pathophysiology in several animal models of atherosclerosis-related diseases [5, 14, 15]. A human clinical trial using BR55 (VEGFR2-targeted MBs) to detect breast and ovarian cancer lesions has been reported, which has confirmed the feasibility and safety of this approach [16].

Although ultrasound molecular imaging of early inflammatory changes of atherosclerosis has been elaborated [9, 10, 17], there still remains a great challenge in increasing targeted MB adhesion efficiency in large arterial vessels [18-21]. To address this issue, scholars attempted to utilize external forces (such as acoustic radiation force [22,23] and magnetic field force [24]) to improve the opportunities for targeted MBs to contact the vascular endothelium. And, some researchers have explored dual-targeted MBs to promote MB adhesion with receptors on the surface of endothelial cells [25, 26]. All of these strategies to some extent improved the capability of ultrasound molecular imaging for disease detection. Considering that selectins may favor leucocytes to arrest and crawl on the surface of endothelial cells, in this study, we attempted to develop a triple-targeted MB (named as MB_{VIS}) by integrating VCAM-1 and ICAM-1 antibodies and synthetic polymeric sialyl Lewis X (sLe^x) onto the MB surface. By mimicking the behavior of leucocytes during inflammation, the triple-targeted MB_{VIS} rapidly and firmly bound the inflammatory endothelium, ultimately improving the diagnosis effect of ultrasound molecular imaging. Also, the potential of assessing the pharmacologic intervention effect with atorvastatin against atherosclerosis was investigated by using the triple-targeted MB_{VIS}.

Materials and Methods

Materials

1,2-distearoyl-sn-glycero-3-phosphatidylcholine (DSPC), 1,2-distearoyl-sn-glycero-3-phosphoethanolamine-N-[methoxy(polyethylene glycol)-2000] (DSPE-PEG2000) and 1,2-distearoyl-sn-glycero-3-phosphoethanolamine-N-[biotinyl(polyethylene glycol)-2000] (DSPE-PEG2000-Biotin) were purchased from Avanti Polar Lipids Inc. (Alabaster, AL, USA). Avidin was obtained from Sigma-Aldrich (St. Louis, MO, USA). Biotinylated anti-mouse CD106 (VCAM-1) antibody was purchased from eBiosciences (San Diego, CA, USA), anti-mouse CD54 (ICAM-1) antibody was from LifeSpan Biosciences Inc. (Seattle, WA, USA), and multivalent biotinylated polymer sialyl Le^x-PAA-biotin was purchased from GlycoTech corporation (Gaithersburg, Maryland, USA). Biotinylated mouse IgG isotype control antibody, Alexa Fluor®647-labeled anti-rabbit IgG antibody and

Alexa Fluor®405-labeled anti-rat IgG antibody were obtained from Abcam Trading (Shanghai) Company Ltd. (Pudong, Shanghai, China), and fluorescein isothiocyanate (FITC)-labeled anti-CD15s antibody was obtained from Santa Cruz Biotechnology Inc. (Dallas, Texas USA). All other reagents were of analytical grade. Mouse brain microvascular endothelial cells (bEnd.3) were purchased from the American Type Culture Collection (Manassas, VA, USA).

Preparation of targeted MBs and control MBs

Biotinylated, lipid-shelled MB (MB_{Biotin}), triple-targeted $MB_{VCAM-1+ICAM-1+sLe^x}$ (MB_{VIS}), six single/dual-targeted MBs including MB_{VCAM-1} (MB_V), MB_{ICAM-1} (MB_I), MB_{sLe^x} (MB_S), $MB_{VCAM-1+ICAM-1}$ (MB_{VI}), $MB_{VCAM-1+sLe^x}$ (MB_{VS}), $MB_{ICAM-1+sLe^x}$ (MB_{IS}) and isotype control MBs (MB_{IgG}) were prepared as previously described [27]. Briefly, DSPC, DSPE-PEG2000 and DSPE-PEG2000-Biotin (molar ratios = 9:0.5:0.5) were dissolved in chloroform. The solvent was then evaporated under nitrogen flow at room temperature, producing a thin layer of phospholipid membrane. After two-hour vacuum treatment, the completely dried phospholipid membrane was hydrated at 60°C with Tris (hydroxymethyl) aminomethane buffer saline, and transferred into vials (1 mL for each). After sealing the vials, perfluoropropane (Flura, Newport, TN, USA) was added. These vials with phospholipid suspension were mechanically vibrated for 30 s. The resulting MB_{Biotin} were rinsed and incubated with avidin. After eliminating free avidin by PBS rinse, these MBs (about 5×10^8) were further incubated with 30 μg biotinylated antibody for the preparation of single-targeted MBs or isotype control MBs. A blend of biotinylated antibodies was used to fabricate the multi-targeted MBs, with 15 μg each for dual-targeted MBs or 10 μg each for triple-targeted MBs.

Characterization of targeted MBs

Fluorophore-labelled targeted MBs were fabricated by incubating with fluorophore-labelled secondary antibodies at room temperature for 20 min, followed by rinsing and removal of the free secondary antibodies. Particle size and size distribution of MBs were measured with Accusizer 780 Optical Particle Sizer (Particle Sizing Systems, Santa Barbara, CA, USA). A drop (about 20 μL) of each kind of fluorophore-labelled targeted MBs suspension was applied to the microscope slide and observed under a fluorescence microscope (Olympus, Tokyo, Japan). The ligand conjugation efficiency of targeted MBs was detected according to the fluorescence intensity of fluorophore-labeled secondary antibodies (against VCAM-1/ICAM-1 antibodies) or anti-CD15s antibodies (against sLe^x polymers) by using Synergy 4 microplate reader (BioTek, Winooski, VT, USA).

In vitro cell static binding assay

The murine bEnd.3 cells were cultured in a 24-well plate (1×10^4 cells per well) overnight in Dulbecco's modified Eagle's medium, supplemented with 10% fetal bovine serum and 1% penicillin-streptomycin solution. The plate was maintained in a humidified atmosphere containing 5% CO_2 at 37°C. When the cells reached 60-70% confluence, 10 ng/mL, 20 ng/mL or 40 ng/mL tumor necrosis factor-α (TNF-α, Novoprotein, Summit, NJ, USA) was added and further incubated for 8 h. The expression levels of VCAM-1, ICAM-1 and P-selectin were detected by flow cytometry. The TNF-α-stimulated bEnd.3 cells were used to test the static adhesion capability of targeted MBs. In brief, cells were stained with DAPI. Then, the medium was removed and 1 mL MBs (1×10^6 bubbles/mL) was added into the TNF-α-stimulated cell monolayer. The cell culture plates were sealed, inverted and rotated for 5 min. After the free MBs were removed by a PBS rinse, the number of attached MBs was determined under an optical microscope (Olympus, Tokyo, Japan) at five random bright fields of view. The result was expressed as the ratio of MBs to cell number in the same field.

Flow chamber studies

The dynamic adhesion efficiency of MBs was determined using a parallel plate flow chamber system (Glycotech, Gaithersburg, MD, USA). Murine bEnd.3 cells were grown to confluence on 35 mm culture dishes and stimulated with TNF-α (40 ng/mL) for 8 h. Cells were stained by DAPI to label the nuclei. Dishes were mounted on a parallel plate flow chamber. A suspension of control or triple-targeted MBs (1×10^6 bubbles/mL) in PBS was drawn through the flow chamber with an adjustable withdrawal pump. The dishes were then removed from the apparatus, rinsed with PBS and imaged immediately with a phase-contrast bright-field microscope (Olympus, Tokyo, Japan, × 400). The MBs attached to cells were counted in five randomly selected optical fields after 4 min continuous flow under 1.0, 2.0, 4.0, 8.0 and 12.0 dyn/cm² shear stress. The adhesion ability of targeted MBs under 4 dyn/cm² shear stresses for 0.5, 1.0, 2.0, 3.0 and 4.0 min was also tested. Each kind of MBs was measured in 3 replicates [10].

Animal model

Five to six-week-old apolipoprotein E-deficient ($ApoE^{-/-}$) mice and wild-type mice (C57BL/6) were obtained from Vital River Laboratory Animal

Technology (Beijing, China). These animals were divided into four different groups: (1) A-HD group, $ApoE^{-/-}$ mice were fed a hypercholesterolemic diet (containing 21% fat and 0.15% cholesterol by weight, n = 20); (2) A-RD group, $ApoE^{-/-}$ mice were fed a regular diet (n =20); (3) C-HD group, C57BL/6 mice were fed a hypercholesterolemic diet (n =20); and (4) C-RD group, C57BL/6 mice were fed a regular diet (n = 20). For the treatment experiments, atorvastatin (0.1% wt/wt, dissolved in sodium carboxymethyl cellulose solution) or placebo (sodium carboxymethyl cellulose solution) was added into the hypercholesterolemic diet of the A-HD mice for 8 weeks (n = 20 for each group).

In vivo ultrasound molecular imaging

Ultrasound molecular imaging was performed at three feeding time points: 6 weeks, 10 weeks and 14 weeks. Mice were kept anesthetized with 2% isoflurane in oxygen (2 L/min) on a heated stage. High frequency ultrasound imaging of the aortic arch in the long axis plane from a right parasternal window was performed with a high resolution ultrasound imaging system equipped with a MS250 nonlinear transducer (Vevo 2100; VisualSonics, Toronto, Canada). All imaging parameters (lateral and axial resolution of 165 μm and 75 μm, respectively; center frequency, 18 MHz; transmit power, 10%; dynamic range, 40 dB) were kept constant. To reduce motion artifact, both the ultrasound probe and the animal were fixed and remained at the same position throughout the image acquisition. 5×10^7 MBs (in 50 μL PBS) were injected into tail veins, followed by flushing with 25 μL PBS. To differentiate the acoustic signal derived from MBs attached to vascular endothelial cells and MBs circulating in the bloodstream, image acquisition and quantification were performed using a well-established protocol [16]. Briefly, after the 4 min waiting period, a series of 500 ultrasonographic frames was acquired with a high-power ultrasound destruction pulse sequence applied for 1 s. In consideration of the animal ethics and possible death from excessive injection, MB_{IgG}, MB_V, MB_{IS} and MB_{VIS}, one after another, were injected into the same mouse. MB_I, MB_S, MB_{VI} and MB_{VS}, one after another, were injected into another mouse in the same group. The order of bubble injection was chosen to minimize potential effects between different MBs. A 30 min interval was maintained between administration of different MBs to ensure bubbles had cleared. In the therapeutic evaluation experiments, MB_{VIS} and MB_{IgG} were used in atorvastatin-treated or placebo-treated mice. The imaging strategy was the same as that described above.

Data analysis of *in vivo* imaging datasets

Data analysis of the imaging data was accomplished using the commercially available Vevo CQ software (VisualSonics, Toronto, Ontario, Canada). The region of interest (ROI) was defined as the ascending aorta including the sinus of valsalva to the brachiocephalic artery. Movement caused by breathing and heart beating was automatically corrected as well. The frames before the destruction pulse represented the bound and circulating MBs, and the images after the destruction pulse corresponded to MBs that were still in circulation. The quantification of signal from attached MBs was expressed as differential targeted enhancement (dTE), which was calculated by subtracting the echo signals averaged in the segment after the destruction pulse from those before the destruction pulse. The dTE was expressed in arbitrary units (a.u.). The results were visually displayed as color-coded maps on contrast-mode images and the scale was kept constant.

Histology

Twelve randomly selected mice with different genetic backgrounds and diets from the 4 groups at 3 time points were euthanized. The mice were perfused with 0.9% saline and underwent perfusion fixation with 4% paraformaldehyde. The aortas were taken and fixed in 4% paraformaldehyde for 48 h. Serial cryosections of the ascending aorta, on the short axis, 6 μm thick, were selected at every 60 μm interval and stained with hematoxylin and eosin (H&E). The intima-media thickness was measured on the H&E stained micrographs at the thickest site of the vessel. Lipid deposition were identified by Oil Red O staining. Additionally, the entire aorta from an A-HD mouse raised for 30 weeks was dissected and stained with Oil Red O.

Immunofluorescence staining

Serial cryosections of the ascending aorta were mounted on glass slides, air-dried, blocked with 10% goat serum in PBS and incubated overnight at 4°C with biotinylated anti-VCAM-1 (1:50 dilution in PBS, eBiosciences), biotinylated anti-ICAM-1 (1:50 dilution in PBS, LifeSpan Biosciences) or FITC-labeled anti-P-selectin (1:50 dilution in PBS, Santa Cruz) antibodies. Avidin-FITC (1:500 dilution in PBS, Sigma) was added to bind to the biotinylated antibodies and incubated for 1 h at 37°C. Sections were imaged using a fluorescence microscope (Olympus, Tokyo, Japan).

Western blotting

The ascending portion of the aorta was homogenized in RIPA lysis buffer (Beyotime,

Shanhai, China) containing Protease Inhibitor Cocktail Set I (Merck, Darmstadt, Germany). The lysates were centrifuged at 16,163 rcf for 15 min at 4°C. A loading buffer (0.5 M Tri-HCl, 10% sodium dodecyl sulfate, 0.5 M DTT, 0.5% bromophenol blue and 50% glycerol, pH 6.8) was added to the lysates. Protein concentration was measured by the Micro BCA (bicinchoninic acid) protein assay kit (Thermo Scientific). 10 μg of protein were resolved on SDS-PAGE and transferred to Polyvinylidene fluoride (PVDF) membranes. After blocked with 5% milk for 1 h at room temperature, the membranes were further incubated with primary rat anti-mouse VCAM-1 antibody (1:200 dilution; eBioscience), rat anti-mouse ICAM-1 antibody (1:200 dilution; Abnova), or rabbit anti-mouse P-selectin antibody (1:200 dilution; Santa Cruz), followed by incubation with the peroxidase-conjugated secondary anti-rabbit or rat IgG (1:5000 dilution; ZSGB-Bio, Beijing, China). As control, the mouse anti-β-actin-HRP antibody (1:10, 000 dilution; Sigma, St. Louis, MO, USA) was also used. The immunoblots were visualized by an enhanced chemiluminescence (ECL) detection system (Pierce, IL, USA). The expression levels were quantified with Image J software. The ratios of VCAM-1, ICAM-1 or P-selectin to corresponding β-actin band density were calculated and expressed as a percentage.

Statistical Analysis

All results are presented as mean ± standard deviation (SD). Statistical comparisons were performed using the SPSS 23.0 software (International Business Machines Corporation, Armonk, NY, USA). Statistical differences of MB characterization and *in vitro* cell adhesion were tested with one-way ANOVA followed by LSD post-hoc test. Statistical differences of ultrasound molecular imaging and immunoblotting band density between groups were tested with 2-sided paired Wilcoxon tests. The differences were considered to be significant if $P < 0.05$.

Results

Preparation and characterization of targeted MBs

A biotin-avidin linkage method was used to construct these targeted MBs, by which avidin and biotinylated ligands were gradually conjugated onto the biotinylated MBs. For the triple-targeted MB (MB_{VIS}), the ligand mixture, including biotinylated anti-VCAM-1 antibodies, anti-ICAM-1 antibodies and sLe^x polymers, was incubated with $MB_{biotin\text{-}avidin}$ (Fig. 1A). Fig. 1B shows a photomicrograph of MB_{VIS} under an inverted microscope with phase contrast. From the image, we can see that there was no conspicuous interconnection between MBs. The typical size distribution of MB_{VIS} is displayed in Fig. 1C, revealing an obvious peak at 1-3 μm. Similarly, the control single- or dual-targeted and isotype MBs were also prepared. The number-weighted diameter of MB_{VIS} and its control MBs are presented in Table S1. Similar diameters could be observed.

To test the successful conjugation of these ligands onto the surface of the MBs,

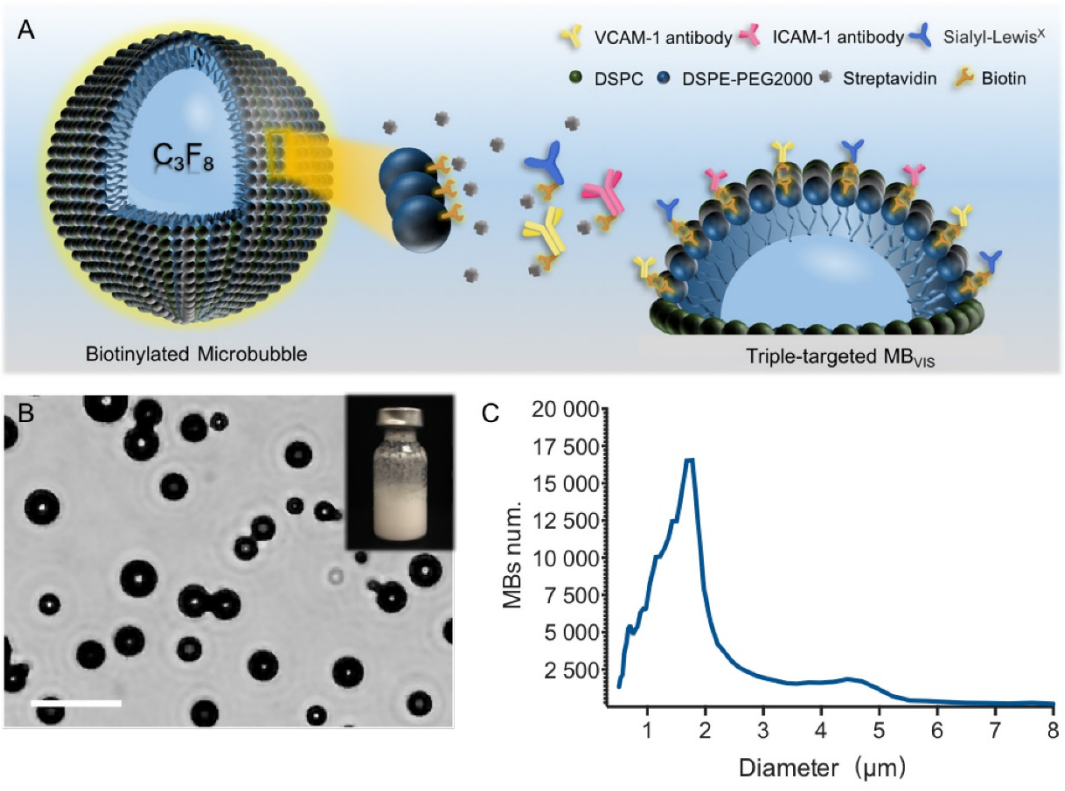

Figure 1. Preparation and characterization of MB_{VIS}. (A) Schematic diagram of targeted MB_{VIS}. (B) Representative photomicrograph of MB_{VIS} (scale bar = 10 μm); inset shows a bottle of MB_{VIS} suspension. (C) The size distribution curve of MB_{VIS} with an obvious peak at 1-3 μm.

fluorophore-labeled antibodies and/or sLe^x polymers were used to fabricate these targeted MBs. Fig. 2 shows representative fluorescence images of seven kinds of fluorophore-labelled targeted MBs. All of them showed fluorescent rings. Labelled MB_V, MB_I and MB_S emitted pure blue, red and green fluorescence, respectively. Labelled MB_{VI}, MB_{VS} and MB_{IS} appeared pink, turquoise and tangerine due to the color merge, respectively. As expected, MB_{VIS} presented the three-mixed color, indicating the successful conjugation of fluorophore-labeled antibodies and polymers. The ligand conjugation efficiencies of the targeted MBs are presented in Table S2, showing a comparable conjugation efficiency for anti-VCAM-1, ICAM-1 antibodies or sLe^x polymers.

In vitro cell adhesion

bEnd.3 cells were used to develop the *in vitro* inflammatory cell model by stimulating with different concentrations of TNF-α. The expression levels of VCAM-1, ICAM-1 and P-selectin were gradually increased with the increase in TNF-α concentration, revealing good linear correlations for VCAM-1, ICAM-1 and P-selectin (Fig. 3A-C). Also, extension of TNF-α incubation time from 4 h to 24 h improved the expression levels of all three factors at all examined TNF-α concentrations (Fig. S1). In order to examine the targeting adhesion of these MBs to the inflammatory cells, bEnd.3 cells stimulated with 40 μg/mL of TNF-α were incubated with these MBs. Fig. 3D shows representative bright-field micrographs of these MBs bound to cells, revealing that these targeted MBs can bind the TNF-α-stimulated cells. The quantitative analysis showed that all of the single- or dual-targeted MBs had stronger binding affinity to stimulated bEnd.3 cells than MB_{IgG} ($P < 0.05$), with 4.75 ± 1.38,4.51 ± 1.22,and 4.39 ± 1.35 bubbles per cell for MB_{VI}, MB_{VS}, and MB_{IS}, while MB_{VIS} showed the highest cell adhesion capability with 12.73 ± 6.05 MBs attached onto the surface of bEnd.3 cells (Fig. 3D, E). Importantly, the number of MB_{VIS} bound to the stimulated cells increased with the increase in TNF-α concentration (Fig. 3F), showing a good linear correlation (Fig. 3G). This result indicated that the cell affinity of MB_{VIS} to the stimulated cells can infer the cell inflammation degree.

In vitro dynamic adhesion of MBs

To further test the dynamic adhesion ability of MB_{VIS}, a parallel plate flow chamber was used to create different flow environments, in which the TNF-α-stimulated bEnd.3 cells were seeded on the bottom of the chamber. Fig. 4A demonstrates MB accumulation under different shear stresses after 4 min MB perfusion. Although the accumulation numbers of all kinds of MBs tended to decrease with the increase in shear stress, the accumulation numbers of MB_{VIS} were always higher than those of single- or dual-targeted MBs under all shear stress ($P < 0.05$). No MB_{IgG} bound onto the stimulated cells at all examined shear stresses. Keeping the shear stress constant at 4 dyn/cm^2, the MB accumulation over time increased gradually (Fig. 4B and Fig. S2). Obviously, the single- or dual-targeted MBs had higher MB accumulation than that of MB_{IgG}, and the triple-targeted MB_{VIS} showed the most significant increase in MB accumulation at different perfusion times ($P < 0.05$).

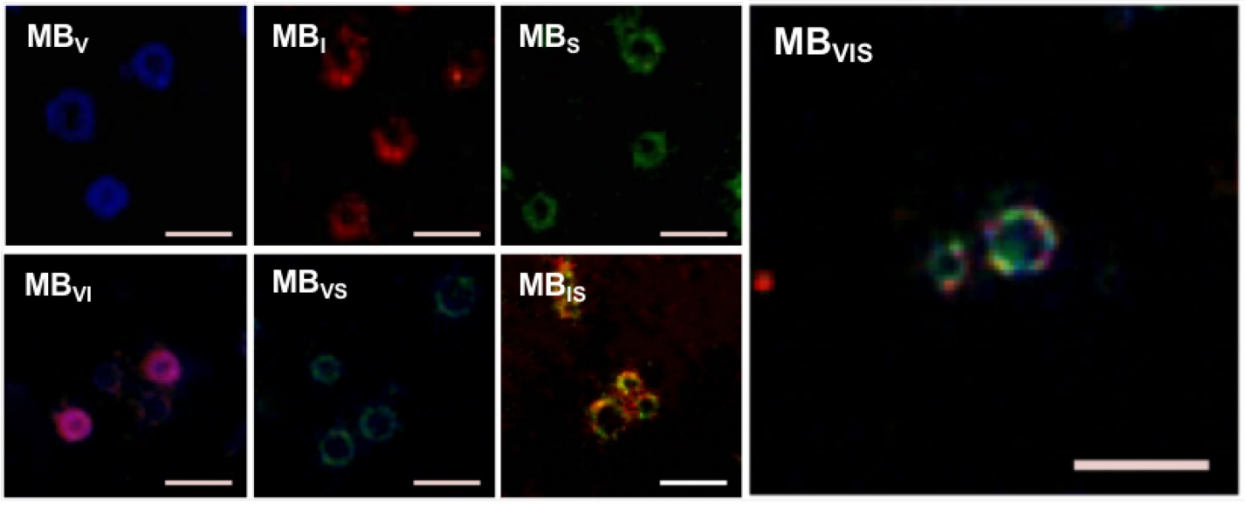

Figure 2. Fluorescence microscopic examination of the fluorophore-labelled targeted MBs. Representative fluorescence micrographs of single-/double-/triple- targeted MBs (scale bar = 10 μm) indicated the successful conjugation of three kinds of ligands to the surface of corresponding MBs.

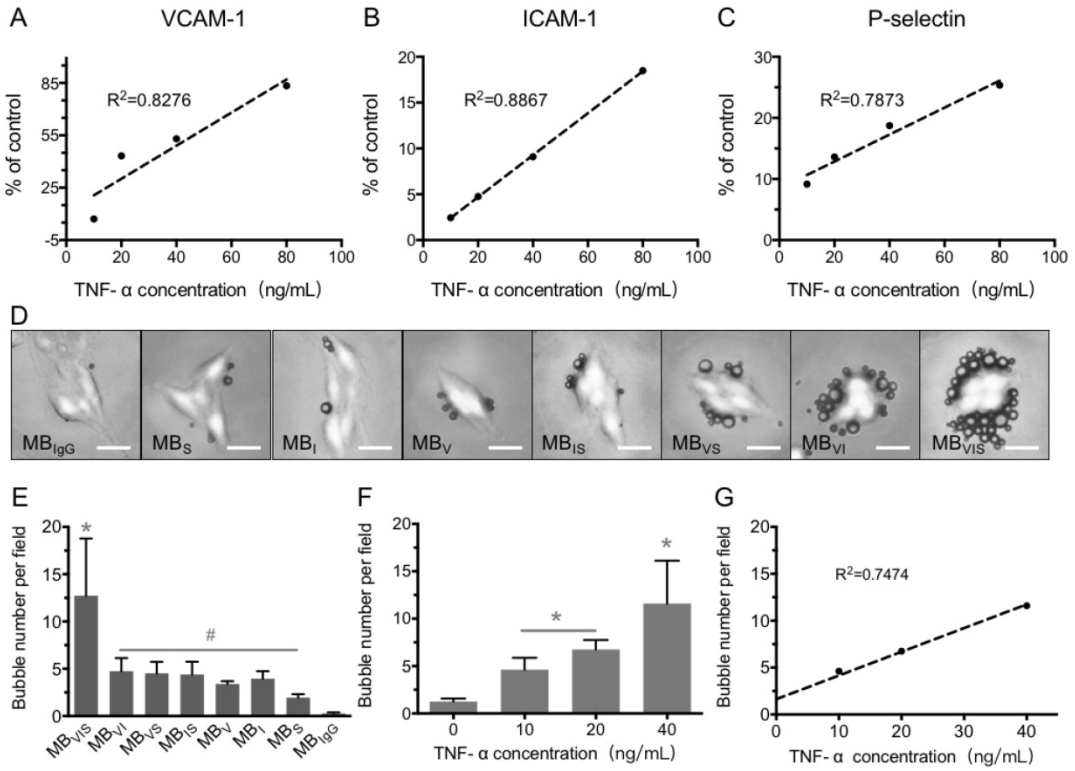

Figure 3. ***In vitro*** **static adhesion of targeted MBs to inflammatory cells.** (A-C) Correlation analysis between the concentrations of TNF-α and the expression levels of VCAM-1, ICAM-1 and P-selectin on bEnd.3 cells stimulated by TNF-α for 8 h. (D) Representative bright-field micrographs of targeted MBs and MB_{IgG} bound to stimulated bEend.3 cells (40 ng/mL TNF-α; scale bar =10 μm). (E) Quantitative assay for the number of MBs adhered onto bEnd.3 cells. #: $P < 0.05$ and *: $P < 0.01$. (F) The number of MB_{VIS} attached to cells stimulated with 0, 10, 20 or 40 ng/mL TNF-α. *: $P < 0.05$. (F) Correlation analysis between the number of attached MB_{VIS} and concentrations of TNF-α used in the stimulation experiment.

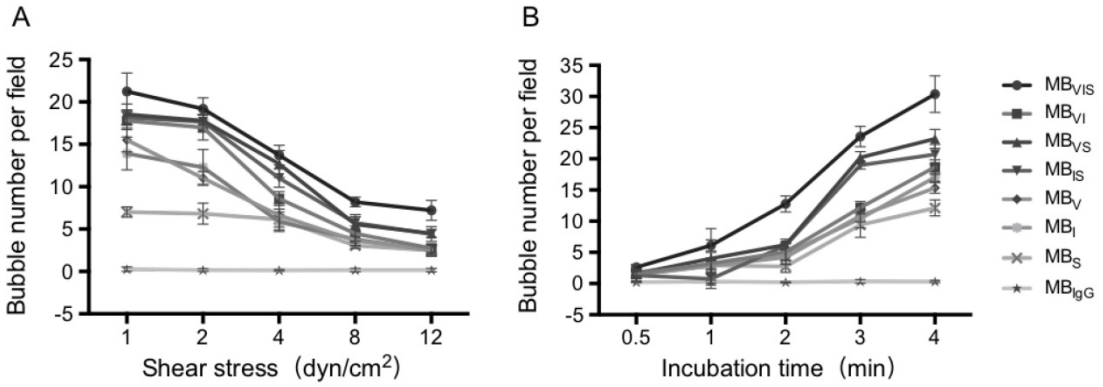

Figure 4. Dynamic adhesion of MBs under the parallel plate flow chamber. (A) The number of MBs bound to the TNF-α-stimulated cells in different flow shear stresses after 4 min. (B) The number of MBs bound to the TNF-α-stimulated cells at different times under 4 dyn/cm² flow shear stress.

In vivo ultrasound molecular imaging

In order to evaluate the capability of these targeted MBs for ultrasound molecular imaging of atherosclerotic plaques, apolipoprotein E-deficient C57BL/6 ($ApoE^{-/-}$) and wild type C57BL/6 mice fed a hypercholesterolemic diet or regular diet were used. Fig. 5A shows representative images folowing intravenous injection of targeted MBs or MB_{IgG} into the $ApoE^{-/-}$ mice fed a hypercholesterolemic diet (A-HD) for 10 weeks. A good signal-enhanced performance of these targeted MBs on ultrasound molecular imaging could be observed. The three single-targeted MBs showed higher mean video intensities than MB_{IgG}, with 13.37 ± 2.54, 12.93 ± 0.76, 14.4 ± 0.7 a.u for MB_V, MB_I and MB_S but only 0.7 ± 0.4 a.u for MB_{IgG}. All three dual-targeted MBs had higher mean video intensities than their corresponding single-targeted MBs, with 26.8 ± 2.66, 21.87 ± 1.1 and 17.67 ± 0.72 a.u for MB_{VI}, MB_{VS} and MB_{IS}, respectively. As expected, triple-targeted MB_{VIS} showed the highest mean video intensity (32.73 ± 1.82 a.u.) among all MBs

(Fig. 5B). Interestingly, the significant advantage of MB_{VIS} over other single/dual-targeted MBs could also be observed at the early stage of atherosclerotic plaque formation in ApoE$^{-/-}$ mice when they were fed a hypercholesterolemic diet for 6 or 14 weeks (Fig. S3). Fig. 5C shows representative color-coded sonographic images from four groups of mice after intravenous injection of MB_{VIS}. Stronger imaging signals could be observed in the A-HD group than in the ApoE$^{-/-}$ mice fed a regular diet (A-RD), C57BL/6 mice fed a hypercholesterolemic diet (C-HD) or C57BL/6 mice fed a regular diet (C-RD) at the same feeding time (all $P < 0.05$). Notably, the difference in enhanced ultrasonic signals became more significant with the increase of feeding time from 6 weeks to 14 weeks (Fig. S3).

In order to validate the results of ultrasonography, ascending aortas of mice were harvested and analyzed by histological examination and western blotting. Fig. 6A, B show representative micrographs of H&E staining from aorta tissue sections of A-HD mice. Intimal thickening and large atherosclerotic plaques protruding into the lumen were seen with the extension of hypercholesterolemic diet feeding time, particularly in the animals fed for 20 weeks (Fig. 6A, B). Oil Red O staining revealed red-stained lipids under the endothelium (Fig. 6C). Giant plaques could be observed in 30-week A-HD mice, which almost occupied the whole lumen area (Fig. 6D). Fluorescence immunohistochemical staining showed a gradually increased expression of VCAM-1, ICAM-1 and P-selectin on endothelium of ascending aorta from A-HD mice with increasing HD feeding time (Fig. 6E). It was further confirmed by western blotting experiments that the expression of these factors in the ascending aortas of A-HD mice was relatively higher than in the other three groups and all of them increased with hypercholesterolemic diet feeding time (Fig. 6F-I). Both the immunohistochemical staining and western blotting results indicate the same tendency, which is similar to the results from ultrasound molecular imaging.

Assessment of atorvastatin efficacy against atherosclerosis

To further test the capability of MB_{VIS} on the assessment of atorvastatin efficacy, we performed ultrasound molecular imaging of the ascending aorta of ApoE$^{-/-}$ mice that received atorvastatin or placebo added into their daily hypercholesterolemic diet. A significantly reduced serum lipid profile including high density lipoprotein cholesterol (HDLC), low density lipoprotein cholesterol (LDLC), triglyceride (TG) and total cholesterol (T-CHO) was found in the A-HD mice that received atorvastatin treatment for 8 weeks (Table S3). H&E staining examination revealed significant intimal thickening in the ascending aorta of placebo-treated A-HD mice, but not in atorvastatin-treated A-HD mice (Fig. 7A, B) ($P<0.05$), demonstrating that addition of atorvastatin could effectively inhibit the progression of atherosclerosis. Fig. 7C, D shows that significantly reduced ultrasound molecular imaging signals appeared in the atorvastatin-treated A-HD mice than in the placebo-treated A-HD mice when using MB_{VIS} ($P < 0.05$). By contrast, no significant change in signal intensity was found between the two groups of animals when MB_{IgG} was used. Immunofluorescence staining and western blotting analysis further confirmed the significantly lower expression of VCAM-1, ICAM-1 and P-selectin on endothelium of ascending aorta of mice treated with atorvastatin for 8 weeks, compared with placebo-treated A-HD mice (Fig. 8). These data indicate MB_{VIS},

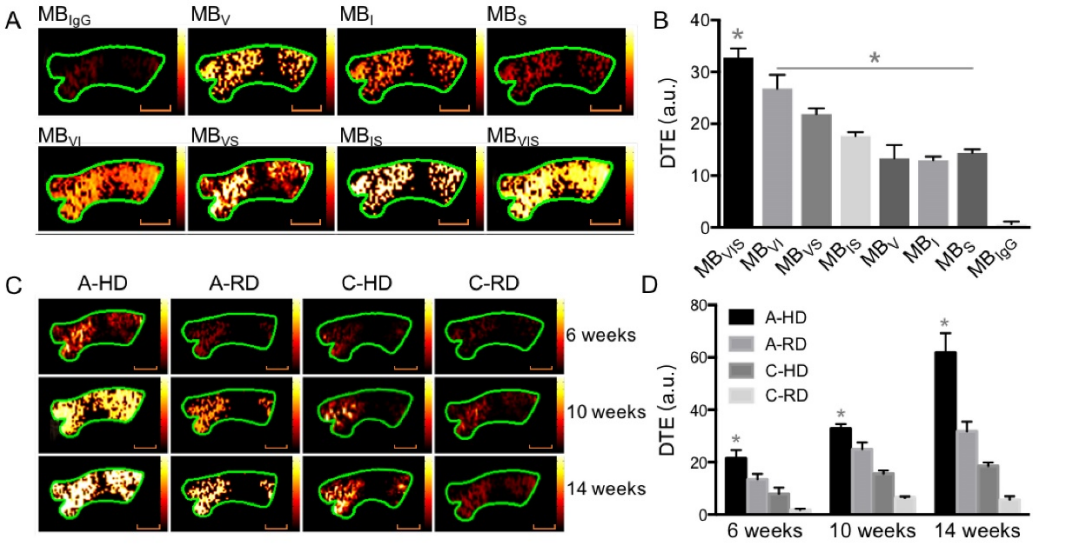

Figure 5. *In vivo* ultrasound molecular imaging of the ascending aorta. (A) Representative color-coded ultrasound images after injection of various kinds of MBs at the 10 week feeding time, and (B) the quantitative analysis of ultrasound signal intensities. *: $P < 0.05$. (C) Representative color-coded images from four groups after injection of MB_{VIS}, and (D) the quantitative analysis of ultrasound signal intensities. Stronger signal could be observed in the A-HD group than in the control groups at the same time. *: $P < 0.05$. Scale bar = 1 mm.

but not MB_{IgG}, can be used as a probe to assess the pharmacologic efficacy at the early stage of atherosclerosis by ultrasound molecular imaging technology.

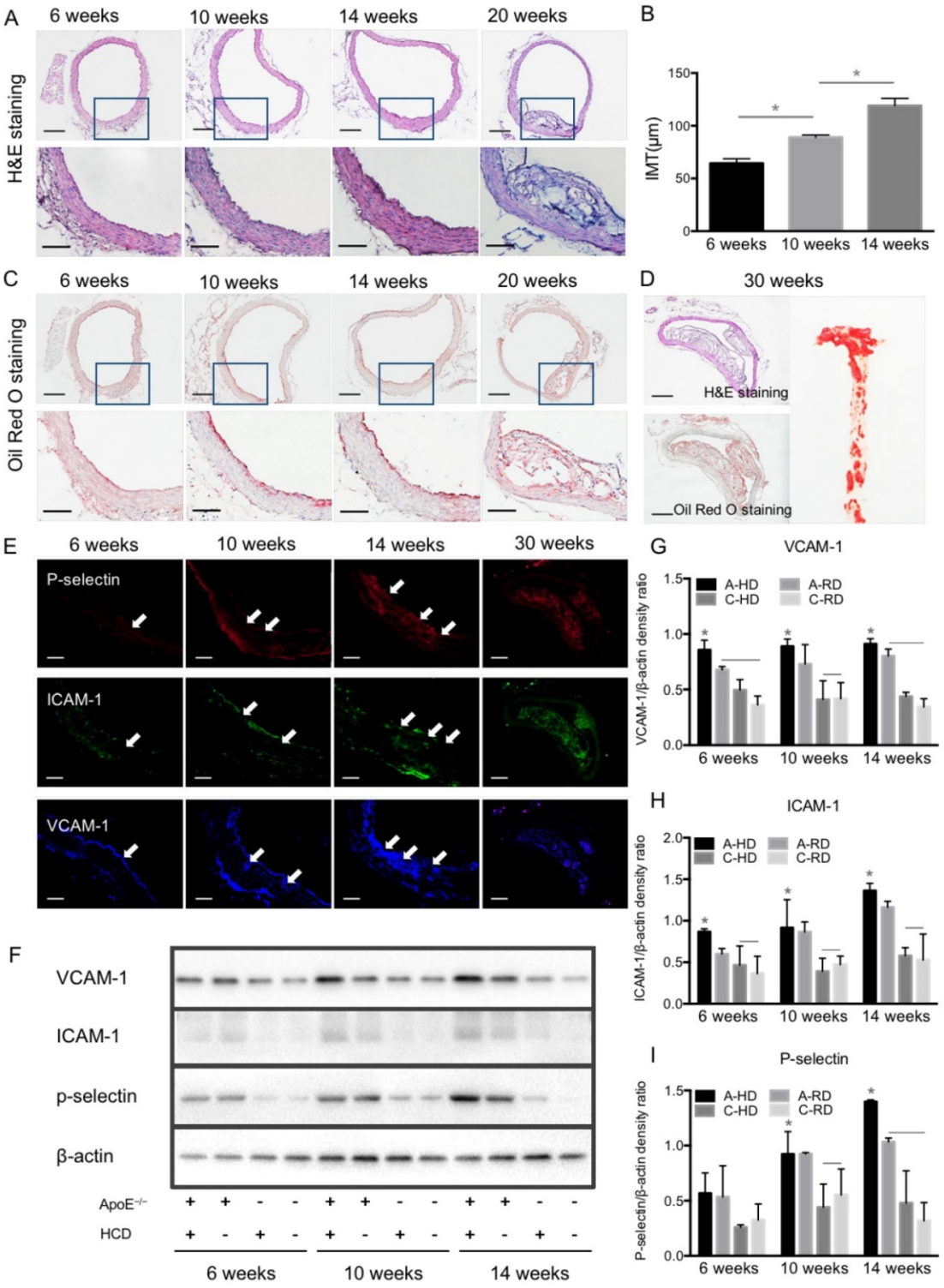

Figure 6. Progression of atherosclerotic plaques and expression of VCAM-1, ICAM-1 and P-selectin. (A) Representative micrographs of H&E-stained aorta sections from ApoE$^{-/-}$ mice fed HD for 6, 10, 14 or 20 weeks. (B) Quantitative analysis of intima-medial thickness. The intima-medial thickness increased with the extension of feeding time. *: $P < 0.05$. Scale bars in micrographs with low magnification are 200μm, and 100μm in micrographs with high magnification. (C) Representative micrographs of aorta sections stained with Oil Red O. An apparent atherosclerotic plaque could be observed at the 20-week HD feeding time. (D) Giant plaques in sections from mice fed 30 weeks occupied almost the whole lumen. (E) Representative micrographs of immunofluorescence staining for VCAM-1, ICAM-1 and P-selectin proteins on endothelium of ascending aorta from A-HD mice. VCAM-1, ICAM-1 and P-selectin were labelled as blue, red and green. Scale bar = 100 μm. (F) Western blotting analysis of the expression of VCAM-1, ICAM-1 and P-selectin from the aorta tissue of A-HD, A-RD, C-HD and C-RD mice fed for 6, 10 or 14 weeks. (G-I) Quantitative analysis of the expression levels of VCAM-1, ICAM-1 and P-selectin. The ratio values of VCAM-1, ICAM-1 or P-selectin were referenced to β-actin protein level. *: $P < 0.05$.

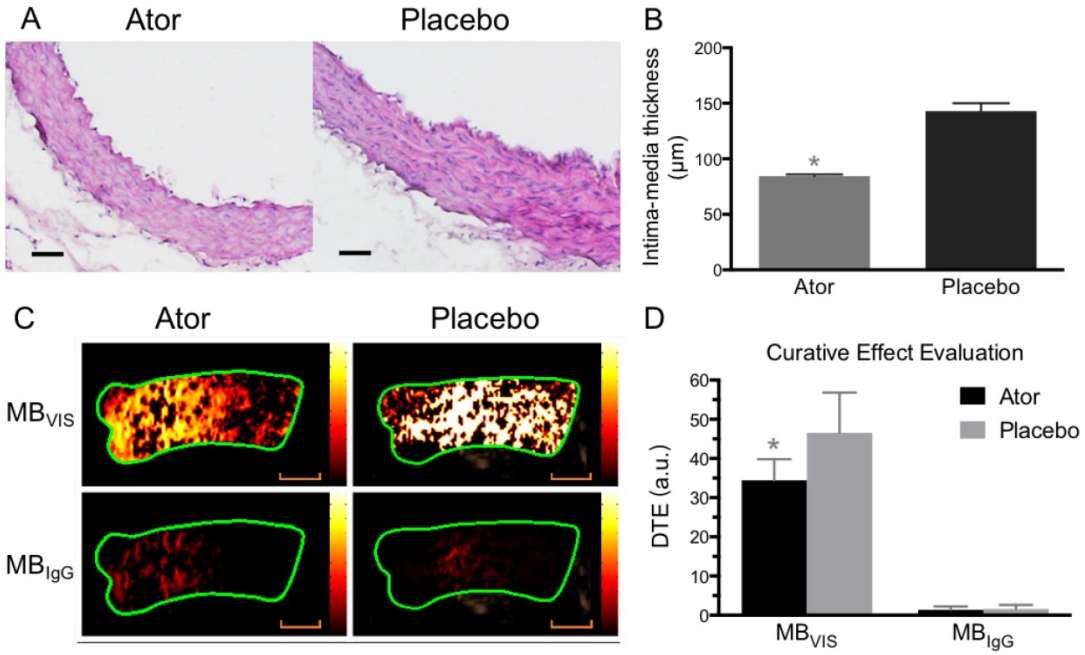

Figure 7. Ultrasound molecular imaging assessment of atorvastatin efficacy. (A) Representative H&E images of ascending aorta sections from ApoE$^{-/-}$ mice fed atorvastatin or placebo in their daily hypercholesterolemic diets for 8 weeks. Scale bar = 50 μm. (B) Quantitative analysis of intima-medial thickness, with reduced intima-medial thickness in the atorvastatin-treated A-HD mice. *: $P < 0.05$. (C) Representative color-coded images of ascending aorta generated from adherent MB_{VIS} or MB_{IgG}. Scale bar = 1 mm. (D) Quantitative analysis of signal intensities from (C). A-HD mice were raised with atorvastatin or placebo added into their daily hypercholesterolemic diet for 8 weeks. *: $P < 0.05$.

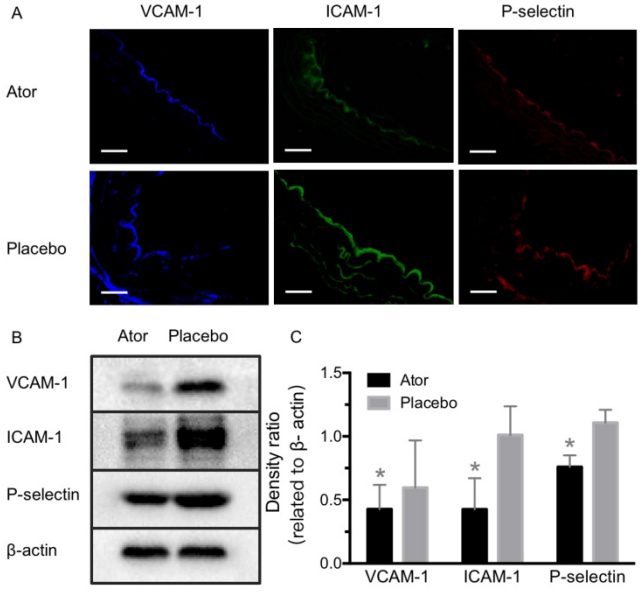

Figure 8. Expression detection of VCAM-1, ICAM-1 and P-selectin after atorvastatin treatment. (A) Representative micrographs of immunofluorescence staining for VCAM-1, ICAM-1 and P-selectin proteins on endothelium of ascending aorta from A-HD mice with atorvastatin or placebo treatment. Scale bar = 100 μm. (B) Western blotting analysis of the expression of VCAM-1, ICAM-1 and P-selectin from the aorta tissue of A-HD mice with atorvastatin or placebo treatment. Significantly reduced expression was found in the atorvastatin-treated animals. *: $P < 0.05$.

Discussion

Atherosclerosis is a progressing chronic disease. Conventional non-invasive (e.g., ultrasound) and invasive (e.g., angiography) imaging tools allow for visualization and localization of advanced atherosclerotic lesions. But, it is often too late for some patients when the lesions are found. The early detection of atherosclerotic lesions before they are morphologically visible is important and helpful for risk stratification and decision-making on intensified secondary prevention strategies.

With the advance of ultrasound molecular imaging technology, great potentials are demonstrated to characterize and image the occurrence and development of diseases on the molecular level. The existing bottlenecks for ultrasound molecular imaging of early atherosclerosis mainly come from two aspects: (1) Similar to erythrocytes *in vivo*, the rheologic behavior of MBs tends to keep them close to the axial center of the bloodstream [28], making them less effective contact with the endothelium [29]. It is true at the early stage when there is no obvious plaque in the lumen. (2) Atherosclerosis often occurs in large and moderate arteries, particularly at the sites of bifurcation where there are high blood shear stresses. In this case, MBs easily dissociate from the endothelia molecular targets, leading to insufficient affinity. To address these issues, in this research, we prepared a triple-targeted MB_{VIS} based on VCAM-1, ICAM-1 and P-selectin by integrating the antibodies of VCAM-1 and ICAM-1 and a ligand of synthetic polymeric sLe^x

onto the MB surface.

During the preparation of targeted MBs, different combinations of antibodies and ligand were pre-mixed at the same concentrations. As was shown in Fig. 2, VCAM-1 and ICAM-1 antibodies and sLe^x ligand were successfully coated onto the MB_{VIS} surface. But, we also found that the antibody and ligand amounts coated onto the shell bubble surface were unequal (Table S2); this can be attributed to their different spatial conformation demands. Interestingly, although the number for each single ligand on the MB_{VIS} was about 3-fold fewer than on their corresponding single-targeted MBs, MB_{VIS} still showed significantly higher adhesion efficiency to inflammatory cells in comparison to the single-targeted MBs. In the static adhesion experiment, the number of MB_{VIS} binding to cells was nearly 3-fold higher than the dual-/single-targeted MBs. In the parallel plate flow chamber experiment, MB_{VIS} also showed greater than 2-fold higher cell-binding performance within a short time (1 min) when compared with dual-/single-targeted MBs.

Previous studies have shown that there is a linear relationship between the number of targeted MBs and the amount of antigens or receptors [30, 31]. This linear trend was also observed in our MB static adhesion experiment. Notably, we found that the number of attached MB_{VIS} was linearly correlated with degree of cell inflammation (Fig. 3). This result, therefore, makes it possible to quantify adhesion molecule expression by means of video intensity from retained targeted MBs *in vivo*. Indeed, a significant ultrasound signal enhancement, approximately 2-fold higher than the single-targeted groups, could be seen on the inflammatory endothelium of early atherosclerosis mice by using the triple-targeted MB_{VIS} (Fig. 5). Given that the enhanced ultrasound signals resulted from more MB_{VIS} adhered to the inflammatory endothelium, it is reasonable that MB_{VIS} is a more suitable ultrasound molecular probe for monitoring the genesis and progression of atherosclerosis.

Evidence has demonstrated that atherosclerosis progression is mainly driven by a disturbed equilibrium of lipid accumulation and chronic inflammation of the vessel wall [32]. In the early stage, inflammation is accompanied by the recruitment and transmigration of leucocytes through the endothelium. The success of adhesion between leucocytes and endothelial cells depends on the successive mediation of adhesion molecules. While endothelial- and platelet-specific E- and P-selectins promote the initial attachment and rolling of circulating leucocytes, fast but unstable tethering is established between leucocytes and endothelial cells by mediation of P-selectin and sialyl-Lewis^x, which is sulfated by P-Selectin Glycoprotein Ligand-1 (PSGL-1). The adhesion molecules ICAM-1 and VCAM-1 mediate the firmer adhesion of leukocytes to the endothelium, allowing for their transmigration. As the up-regulation of the adhesion molecules is induced by inflammatory cytokines such as TNF-α (tumor necrosis factor-α) and interleukins [33], and no/less constitutive expression could be detected in normal tissue, these adhesion molecules represent prominent targets for molecular imaging of inflammation-associated processes [13]. Some single-targeted molecular probes targeting biomarkers such as VCAM-1 [10, 11] and P-selectin have been developed for ultrasound imaging of atherosclerosis in genetically modified mouse models. Moderate improvements in adherence efficiency for dual-targeted MBs in combination with adhesion molecules have been reported [17]. By contrast, MB_{VIS} integrating VCAM-1 and ICAM-1 antibodies, and polymeric sLe^x ligand performed more like a leukocyte and produced more significant enhancement of ultrasound imaging signals.

As an extending application, we examined the capability of MB_{VIS} for evaluating pharmacotherapy via ultrasound molecular imaging. Atorvastatin was selected in our study since it is one of the most commonly used clinical drugs for atherosclerosis treatment. As expected, significantly reduced ultrasound imaging signals were observed in the atorvastatin-treated A-HD mice than in the placebo-treated A-HD mice when using MB_{VIS} (Fig. 7). Indeed, atorvastatin treatment reduced vascular inflammation and the expression of VCAM-1, ICAM-1 and P-selectin on the vascular endothelium (Fig. 8), indicating that MB_{VIS} can be used as a tool to evaluate atorvastatin efficacy at the early stage of atherosclerosis.

There are several limitations to our study. The use of avidin-biotin coupling is unlikely to be applied in humans. Future studies will focus on developing contrast agents through a covalent linkage method. Also, we only detected the expression level of P-selectin in the histological analysis. Actually, sLe^x ligand can bind not only P-selectin, but also E-selectin and L-selectin under appropriate conditions. Furthermore, E-selectin and P-selectin bind to sLe^x in a very similar manner, and all of these selectins are important in leukocyte adhesion and atherosclerosis: L-selectin is constitutively expressed on leukocytes; P-selectin appears very rapidly on the endothelial cell surface in response to inflammatory stimuli; E-selectin is expressed by cells undergoing inflammation, and appears on the cell surface after a significant delay [34]. In addition, although our data

from mice did not really prove the applicability of the presented MBs in humans because there are variations in blood shear stresses in humans vs. small animals, our results provide a standard universal technique for our proof-of-principle studies. In theory, stronger attachment efficiency for MB_{VIS} would be achieved since the shear stress is lower in human large arteries than those of mice. Still, it has a long way to go for clinical application.

Conclusions

We have developed a triple-targeted MB_{VIS} by integrating VCAM-1 and ICAM-1 antibodies and synthetic polymeric sLe^x onto the MB surface. MB_{VIS} has good affinity with inflammatory endothelium, giving it significant advantages over its single-targeted or dual-targeted control MBs as a molecular imaging probe to monitor AS genesis and development or to assess pharmacologic interventions. Our study provides a novel probe that can be used for ultrasound molecular imaging for the diagnosis and treatment of atherosclerosis.

Abbreviations

CAM: cell adhesion molecule; MB: microbubble; VCAM-1: vascular cell adhesion molecule 1; ICAM-1: intercellular adhesion molecule 1; sLe^x: sialyl Lewis X; PSGL-1: P-selectin glycoprotein ligand-1; VLA-4: very late antigen-4; MRI: magnetic resonance imaging; PET: positron emission tomography; SPECT: single-photon emission computed tomography; DSPC: 1,2-distearoyl-sn-glycero-3-phosphatidylcholine; DSPE-PEG2000: 1,2-distearoyl-sn-glycero-3-phosphoethanolamine-N-[methoxy(polyethylene glycol)-2000]; DSPE-PEG2000-Biotin: 1,2-distearoyl-sn-glycero-3-phosphoethanolamine-N-[biotinyl(polyethylene glycol)-2000]; FITC: fluorescein isothiocyanate; MB_{Biotin}: Biotinylated lipid-shelled MB; MB_{VIS}: triple-targeted $MB_{VCAM-1+ICAM-1+sLe^x}$; MB_V: MB_{VCAM-1}; MB_I: MB_{ICAM-1}; MB_S: MB_{sLe^x}; MB_{VI}: $MB_{VCAM-1+ICAM-1}$; MB_{VS}: $MB_{VCAM-1+sLe^x}$; MB_{IS}: $MB_{ICAM-1+sLe^x}$; DAPI: 4',6-diamidino-2-phenylindole; ApoE: apolipoprotein E; A-HD: $ApoE^{-/-}$ mice fed with a hypercholesterolemic diet; A-RD: $ApoE^{-/-}$ mice fed with a regular diet; (3) C-HD: C57BL/6 mice fed with a hypercholesterolemic diet; C-RD: C57BL/6 mice fed with a regular diet; dTE: differential targeted enhancement; H&E: hematoxylin and eosin; PVDF: polyvinylidene fluoride; ECL: enhanced chemiluminescence; HDLC: high density lipoprotein cholesterol; LDLC: low density lipoprotein cholesterol; TG: triglyceride; T-CHO: total cholesterol.

Acknowledgments

The authors gratefully acknowledge the support of this research by National Key Basic Research Program of China (973 Program, Grant No. 2015CB755500, 2014CB744502), National Nature Science Foundation of China (Grant No. 81571690,11534013, 81571701, 11325420, 81527901), Key Laboratory for Magnetic Resonance and Multimodality Imaging of Guangdong Province (Grant No. 2014B030301013), Natural Science Foundation of Guangdong Province (Grant No. 2014A030312006), and Shenzhen Science and Technology Innovation Committee (Grant No. JCYJ201704131222613, GJHS20160331194306254, JCYJ20170307165254568).

Supplementary Material

Supplementary figures and tables.
http://www.thno.org/v08p1879s1.pdf

Competing Interests

The authors have declared that no competing interest exists.

References

1. Murray CJ, Vos T, Lozano R, Naghavi M, Flaxman AD, Michaud C, et al. Disability-adjusted life years (DALYs) for 291 diseases and injuries in 21 regions, 1990-2010: a systematic analysis for the Global Burden of Disease Study 2010. Lancet. 2012;380:2197-223.
2. Lusis AJ. Cardiovascular disease genes come together. Atherosclerosis. 2015; 242:630-1.
3. Ross R. Atherosclerosis--an inflammatory disease. N Engl J Med. 1999; 340:115-26.
4. Fenyo IM, Gafencu AV. The involvement of the monocytes/macrophages in chronic inflammation associated with atherosclerosis. Immunobiology. 2013; 218:1376-84.
5. Libby P, Ridker PM, Hansson GK. Progress and challenges in translating the biology of atherosclerosis. Nature. 2011; 473:317-25.
6. McEver RP. Selectins: initiators of leucocyte adhesion and signalling at the vascular wall. Cardiovasc Res. 2015;107:331-9.
7. Kuwano Y, Spelten O, Zhang H, et al. Rolling on E- or P-selectin induces the extended but not high-affinity conformation of LFA-1 in neutrophils. Blood. 2010; 116: 617-24.
8. Shi C, Pamer EG. Monocyte recruitment during infection and inflammation. Nat Rev Immunol. 2011; 11:762-74.
9. Khanicheh E, Qi Y, Xie A, Mitterhuber M, Xu L, Mochizuki M, et al. Molecular imaging reveals rapid reduction of endothelial activation in early atherosclerosis with apocynin independent of antioxidative properties. Arterioscler Thromb Vasc Biol. 2013; 33:2187-92.
10. Kaufmann BA, Sanders JM, Davis C, Xie A, Aldred P, Sarembock IJ, et al. Molecular imaging of inflammation in atherosclerosis with targeted ultrasound detection of vascular cell adhesion molecule-1. Circulation. 2007;116:276-84.
11. Nahrendorf M, Jaffer FA, Kelly KA, Sosnovik DE, Aikawa E, Libby P, et al. Noninvasive vascular cell adhesion molecule-1 imaging identifies inflammatory activation of cells in atherosclerosis. Circulation. 2006;114:1504-11.
12. Rodriguez-Porcel M, Wu JC. Cardiovascular molecular imaging as a tool to study biology. Theranostics. 2013;3:914-5.
13. Kiessling F, Fokong S, Bzyl J, Lederle W, Palmowski M, Lammers T. Recent advances in molecular, multimodal and theranostic ultrasound imaging. Adv Drug Deliv Rev. 2014;72:15-27.
14. Wang X, Hagemeyer CE, Hohmann JD, Leitner E, Armstrong PC, Jia F, et al. Novel single-chain antibody-targeted microbubbles for molecular ultrasound imaging of thrombosis: validation of a unique noninvasive method for rapid and sensitive detection of thrombi and monitoring of success or failure of thrombolysis in mice. Circulation. 2012;125:3117-26.
15. Liu Y, Davidson BP, Yue Q, Belcik T, Xie A, Inaba Y, et al. Molecular imaging of inflammation and platelet adhesion in advanced atherosclerosis effects of

antioxidant therapy with NADPH oxidase inhibition. Circ Cardiovasc Imaging. 2013;6:74-82.
16. Willmann JK, Bonomo L, Carla Testa A, Rinaldi P, Rindi G, Valluru KS, et al. Ultrasound molecular imaging with BR55 in patients with breast and ovarian lesions: first-in-human results. J Clin Oncol. 2017;35:2133-40.
17. Kaufmann BA, Carr CL, Belcik JT, Xie A, Yue Q, Chadderdon S, et al. Molecular imaging of the initial inflammatory response in atherosclerosis: implications for early detection of disease. Arterioscler Thromb Vasc Biol. 2010;30:54-9.
18. Dayton PA, Rychak JJ. Molecular ultrasound imaging using microbubble contrast agents. Front Biosci. 2007;12:5124-42.
19. Bachmann C1, Klibanov AL, Olson TS, Sonnenschein JR, Rivera-Nieves J, Cominelli F, et al. Targeting mucosal addressin cellular adhesion molecule (MAdCAM)-1 to noninvasively image experimental Crohn's disease. Gastroenterology. 2006;130:8-16.
20. Wang S, Unnikrishnan S, Herbst EB, Klibanov AL, Mauldin FW Jr, Hossack JA. Ultrasound molecular imaging of inflammation in mouse abdominal aorta. Invest Radiol. 2017;52:499-506.
21. Rychak JJ, Klibanov AL, Hossack JA. Acoustic radiation force enhances targeted delivery of ultrasound contrast microbubbles: *in vitro* verification. IEEE Trans Ultrason Ferroelectr Freq Control. 2005;52:421-33.
22. Rychak JJ, Klibanov AL, Ley KF, Hossack JA. Enhanced targeting of ultrasound contrast agents using acoustic radiation force. Ultrasound Med Biol. 2007;33:1132-9.
23. Liu J, Zhang P, Liu P, Zhao Y, Gao S, Tan K, et al. Endothelial adhesion of targeted microbubbles in both small and great vessels using ultrasound radiation force. Mol Imaging. 2012;11:58-66.
24. Wu J, Leong-Poi H, Bin J, Yang L, Liao Y, Liu Y, et al. Efficacy of contrast-enhanced US and magnetic microbubbles targeted to vascular cell adhesion molecule-1 for molecular imaging of atherosclerosis. Radiology. 2011;260:463-71.
25. Ferrante EA, Pickard JE, Rychak J, Klibanov A, Ley K. Dual targeting improves microbubble contrast agent adhesion to VCAM-1 and P-selectin under flow. J Control Release. 2009;140:100-7.
26. Weller GE, Villanueva FS, Tom EM, Wagner WR. Targeted ultrasound contrast agents: *in vitro* assessment of endothelial dysfunction and multi-targeting to ICAM-1 and sialyl Lewisx. Biotechnol Bioeng. 2005;92:780-8.
27. Yan F, Li X, Jin Q, Chen J, Shandas R, Wu J, et al. Ultrasonic imaging of endothelial CD81 expression using CD81-targeted contrast agents in *in vitro* and *in vivo* studies. Ultrasound Med Biol. 2012; 38: 670-80.
28. Lindner JR, Song J, Jayaweera AR, Sklenar J, Kaul S. Microvascular rheology of Definity microbubbles after intra-arterial and intravenous administration. J Am Soc Echocardiogr. 2002;15:396-403.
29. Sanz J, Fayad ZA. Imaging of atherosclerotic cardiovascular disease. Nature. 2008;451:953-7.
30. Takalkar AM, Klibanov AL, Rychak JJ, Lindner JR, Ley K. Binding and detachment dynamics of microbubbles targeted to P-selectin under controlled shear flow. J Control Release. 2004;96:473-82.
31. Rychak JJ, Lindner JR, Ley K, Klibanov AL. Deformable gas-filled microbubbles targeted to P-selectin. J Control Release. 2006;114:288-99.
32. Wildgruber M, Swirski FK, Zernecke A. Molecular imaging of inflammation in atherosclerosis. Theranostics. 2013;3:865-84.
33. Simon SI, Green CE. Molecular mechanics and dynamics of leukocyte recruitment during inflammation. Annu Rev Biomed Eng. 2005;7:151-85.
34. McEver RP, Zhu C. Rolling cell adhesion. Annu Rev Cell Dev Biol. 2010; 26:363-96.